Journal of Materials Chemistry C

ROYAL SOCIETY OF CHEMISTRY

PAPER

View Article Online
View Journal | View Issue

Cite this: J. Mater. Chem. C, 2025, 13, 4078

Fabrication of $CuInS_2$/ZnS quantum dot nanocomposite films and investigation of their influence on performance of soda glass-based luminescent solar concentrators†

Yu Imakiire, Yoshiki Iso * and Tetsuhiko Isobe *

The power generation performance of luminescent solar concentrators (LSCs) is decreased by unignorable optical losses including self-absorption of luminescence by the phosphor and optical absorption by the light guide plate. To address the optical loss due to self-absorption, this research focused on the use of core/shell $CuInS_2$ (CIS)/ZnS quantum dots (QDs) with a large Stokes shift. The QDs were dispersed in ethylene-vinyl acetate (EVA) copolymer to fabricate transparent fluorescent nanocomposite films. LSCs were prepared with the nanocomposite films and soda glass plate, a common building material to investigate the effect of optical absorption by the light guide plate on the power generation performance. Synthesized QDs showed yellow emission at 587 nm with a high photoluminescence quantum yield (PLQY) of 61.1%, and their large Stokes shift of 0.82 eV reduced self-absorption, making them suitable for LSC applications. We evaluated the effects of QD concentration, film thickness, light guide plate material, and film position on the performance of the LSCs. Optimized performance was observed at a QD concentration of 6.2 wt% and film thickness of 324 μm, showing 1.71-fold higher photocurrent and 3.58-fold larger area of incident photon-to-current efficiency spectrum compared to without film. Replacing soda glass with low-absorption white glass increased power generation by fourfold. This reveals the significant absorption losses of the PL and scattered incident light by soda glass. Despite the considerable optical loss, soda glass is a necessary component in a light guide plate to promote the use of LSCs as building materials. Our findings indicate that QDs with a narrow emission peak at ~520 nm are required to minimize the absorption loss by soda glass.

Received 12th November 2024,
Accepted 5th January 2025

DOI: 10.1039/d4tc04797d

rsc.li/materials-c

1. Introduction

A luminescent solar concentrator (LSC) is a transparent solar panel using fluorescent materials. This device has the potential to help solve energy problems by generating electricity in vast areas where conventional photovoltaics cannot be installed. The use of a transparent wavelength conversion film containing fluorescent materials enables the construction of LSCs by combining a light guide plate and a solar cell. When the sunlight is irradiated to the wavelength conversion film, a part of the sunlight is scattered and absorbed by the fluorescent materials. The absorbed light is converted into isotropic light with a specific wavelength. The scattered light and the emitted fluorescence are concentrated at the edge of the light guide plate by the total reflection and converted into electricity by the solar cell attached.[1] The advantages of this device are that no cooling system is required as sunlight is not directly irradiated to the solar cell, the arbitrary size of the light guide plate allows a large light receiving area, and the small size of the solar cell leads to resource saving. With these features, the LSC is expected to be applied to building-integrated photovoltaics, such as power generation using large-area window materials.[2–5] However, when LSCs are applied to building window materials with large size scales, the optical path length for the light to reach the solar cell increases. Therefore, losses in the waveguide, such as self-absorption due to the overlap of the absorption and fluorescence peaks of the phosphor and optical absorption by the light guide plate, become prominent. This is one of the critical issues to be solved for the practical application of the large-area LSC.[6,7]

Since organic phosphors are easily decomposed by ultraviolet (UV) light in the sunlight, inorganic phosphors with superior durability have attracted attention for the LSC. Based on the Rayleigh's theory, light scattering intensity is proportional to the sixth power of the particle diameter. Nanocomposite films

Department of Applied Chemistry, Faculty of Science and Technology, Keio University, 3-14-1 Hiyoshi, Kohoku-ku, Yokohama 223-8522, Japan.
E-mail: iso@applc.keio.ac.jp, isobe@applc.keio.ac.jp; Fax: +81 45 566 1551; Tel: +81 45 566 1558, +81 45 566 1554

† Electronic supplementary information (ESI) available. See DOI: https://doi.org/10.1039/d4tc04797d

dispersing nanophosphors in a matrix exhibit high optical transparency;[8,9] thereby, nanophosphor-based LSCs have the great potential to be utilized in the development of transparent solar harvesting panels. Quantum dot (QD) phosphors have attracted much interest as a means of configuring LSCs due to their tunable band gap (E_g) by the quantum size effect, high PL quantum yield (PLQY), and excellent chemical stability by surface modification.[10–13] Especially, QDs with a wide range of absorption wavelengths, large absorption coefficients, and tunable absorption and emission peaks from visible to near UV region are promising for the LSC application.

Fluorescent QDs such as II–VI groups and halide perovskites nanocrystals have been investigated for LSC applications.[14] However, their toxicity and self-absorption of emission are significant problems.[15] We have focused on core/shell $CuInS_2$ (CIS)/ZnS QD which has been developed as an alternative to these QDs in optoelectronic devices.[16–24] The formation of the ZnS shell on the CIS core enhances PLQY through surface passivation to reduce defects that cause non-radiative relaxation. CIS/ZnS QD is a promising material for the LSC application due to its low toxicity, high PLQY,[25] and large Stokes shift.[26] We have previously investigated the application of CIS/ZnS QDs and $CuGaS_2$/ZnS QDs as spectral shifters to improve the spectral sensitivity of a crystalline silicon (c-Si) solar module.[27,28] The results showed the influence of their photoluminescence (PL) properties on the power generation performance.

In order to realize the large-area LSC with excellent power generation performance, it is necessary to investigate the loss due to the optical absorption by the light guide plate. Light guide plate material options for the LSC include optical crystal, glass, and acrylic materials. As with normal window glass, economic factors such as weight, durability and raw material costs must be taken into account when selecting the light guide plate materials for the practical LSC.[29] Glass plates are suitable for use in building materials. Glass materials with a lower concentration of impurity ions, such as quartz glass and white plate glass, exhibit high transparency. However, these materials are expensive and not desired for widespread use. Soda glass is commonly used as window material in buildings because it is easy to process, inexpensive and durable. However, the Fe^{3+} and Fe^{2+} impurities show optical absorption in the near-UV, visible, and the near-infrared regions, which are important for the power generation in the solar cell placed at the edge. As the optical path length increases, the absorption loss of both PL and scattered incident light increases, and the power generation performance of the LSC decreases.[30] When glass was used in an LSC with the optical path length of 1 m, it was reported that the optical efficiency decreased by $\sim$1/2 as its absorbance in the near-infrared region was increased by a factor of $\sim$4.[31]

Our previous work on spectral shifters using CIS/ZnS QDs mentioned above only demonstrated their applicability to the luminescent downshifting technique.[27] In this research, we synthesized CIS/ZnS QDs with a large Stokes shift to address the PL self-absorption loss, and optimized QD nanocomposite film for the LSC application. We fabricated unique LSCs with a long optical path length that are strongly affected by the absorption of the light guide plate, and compared different light guide plate materials and film positions to address the light absorption loss by soda glass. The entire process is summarized in Scheme 1. Core/shell CIS/ZnS QDs were synthesized by the hot-injection method and dispersed in ethylene-vinyl acetate (EVA) copolymer resins to prepare QDs@EVA film samples.[27] Experimental LSCs were fabricated by combining a c-Si solar cell module and a soda glass plate to evaluate the power generation performance. After optimizing QD concentration and thickness of the film, the light guide plate materials and film position for the LSC were varied for comparison.

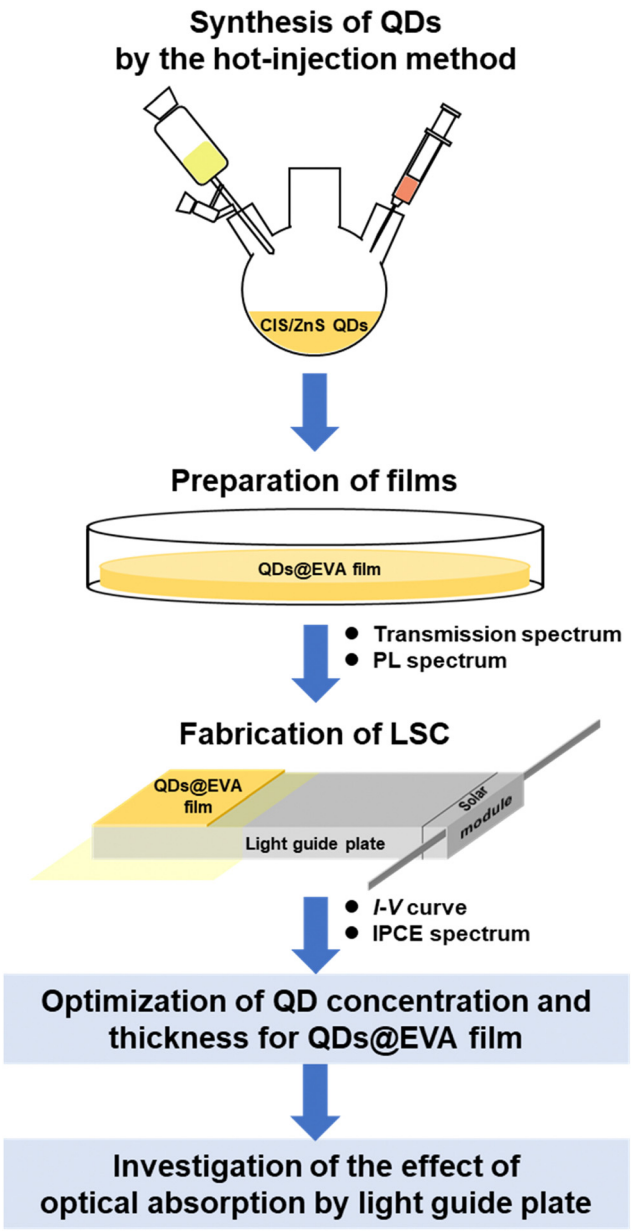

Scheme 1 Schematic procedure of experiments and evaluations.

2. Experimental section

2.1 Materials

Zinc(II) acetate dihydrate (99.999%), copper(I) iodide (99.999%) and indium(III) acetate (99.99%) was purchased from

Sigma-Aldrich. Oleic acid (>85.0%), 1-dodecanethiol (DDT; >95.0%), and 1-octadecene (ODE; >90.0%) were purchased from Tokyo Chemical Industry. Toluene (>99.5%) and ethanol (>99.5%) were purchased from Kanto Chemical. Oleylamine (80–90%) was purchased from Thermo Scientific Chemicals. Sulfur powder (>99.999%) was purchased from Mitsuwa Pure Chemical. Granular EVA copolymer (Evaflex EV150) was purchased from DuPont–Mitsui Polychemicals. Toluene and ethanol were dehydrated over molecular sieves (3A 1/8, FUJIFILM Wako Pure Chemical) prior to use.

2.2 Preparation of QDs

A mixture of zinc(II) acetate dihydrate (4.00 mmol), oleic acid (1.5 mL), DDT (1.0 mL), and ODE (4.0 mL) was heated at 190 °C for 5 min. The mixture was then bubbled with Ar for 30 min to yield a ZnS shell stock solution. Herein, the two solutions were prepared for the double shelling process. A mixture of sulfur powder (0.500 mmol) and oleylamine (5.0 mL) was heated at 100 °C for 20 min, followed by Ar gas bubbling for 30 min to yield a sulfur stock solution. Oleic acid (1.5 mL), DDT (1.0 mL) and ODE (4.0 mL) were placed in a four-necked flask and bubbled with Ar for 30 min. Copper(I) iodide (0.05 mmol) and indium(III) acetate (0.500 mmol) were then added to a four-necked flask. The ZnS shell stock solution was placed in a pressure equalizing dropping funnel connected to the four-necked flask. The system was degassed at 100 °C for 30 min under vigorous stirring and then purged with Ar gas, followed by an increase in the temperature to 150 °C. The sulfur stock solution (3.0 mL) was injected swiftly into the four-necked flask, and the mixture was maintained at 150 °C for 5 min to grow CIS core QDs. One of the ZnS shell stock solutions was then added here at a rate of 1.0 mL min^{-1}. This suspension was heated up to 250 °C and then aged for 50 min for the first shell growth. Another ZnS shell stock solution in a syringe was injected at a rate of 1.0 mL min^{-1}, followed by heating at 250 °C for 60 min. After cooling the suspension of CIS/ZnS core/shell QDs to room temperature, the precipitate was dispersed by adding toluene (7.5 mL) under ultrasonication, followed by addition of ethanol (20.0 mL). The resulting dispersion was centrifuged at ~7000*g* (8000 rpm using a rotor of 10 cm in radius) for 10 min. The supernatant was discarded. The obtained precipitate was redispersed into toluene (5.0 mL) under ultrasonication. After adding ethanol (15.0 mL), the precipitate was collected by centrifugation at ~16 000 *g* (12 000 rpm using a rotor of 10 cm in radius) for 15 min. This washing cycle of redispersion and centrifugation was performed twice. The resulting precipitate was dried in a vacuum desiccator overnight to obtain a solid sample. The QDs were redispersed in toluene to prepare a QD dispersion for measurements.

2.3 Fabrication of QDs@EVA films

A mixture of granular EVA (1.04 g), toluene (12.0 mL), and ODE (600 μL) was stirred for 5 h to prepare the EVA solution. The QD solid samples (50 mg, 100 mg, 150 mg and 200 mg) were dispersed to the EVA solutions under ultrasonication. After Ar gas bubbling for 30 min, the resulting QD dispersions were stirred for 30 s and defoamed for 30 s by using a planetary centrifugal mixer (Thinky, AR-100). The resulting dispersions (3 mL, 5 mL, 7 mL, 9 mL and 11 mL) were dropped on a Petri dish and dried overnight under ambient conditions to fabricate QDs@EVA films. The estimated QD concentrations for the nanocomposite films were 3.2 wt%, 6.2 wt%, 9.0 wt%, and 11.7 wt% depending on the used amount of QD solid sample. The film thicknesses were 79 μm, 164 μm, 233 μm, 324 μm and 373 μm depending on the dropped amount of the dispersion. A blank EVA film without QDs was also prepared in the same manner for comparison. The dried films were cut into a square piece (35 mm × 35 mm) for the LSC application.

2.4 Fabrication of LSC

The LSC was fabricated by attaching a commercial c-Si solar module (35 mm × 10 mm, KSI) to the edge of a glass substrate as a light guide plate (100 mm × 35 mm × 10 mm) (see Fig. S1, ESI†). All areas except the window (35 mm × 35 mm) were covered with Al adhesive tape. White glass and soda glass plates were used for the light guides. A film sample was mounted on the window. The original spectral sensitivity of the c-Si solar module used is shown in Fig. S2 (ESI†).

2.5 Characterization

Powder X-ray diffraction (XRD) profiles were obtained by using an X-ray diffractometer (MiniFlex600, Rigaku) equipped with a Cu Kα radiation source. QD morphology was observed with a field emission transmission electron microscope (FE-TEM; FEI, Tecnai G2). FE-TEM sample for dispersion was prepared by drying a drop of the toluene dispersion of QDs on a molybdenum grid with a collodion film (Oken Shoji, COL-M15). FE-TEM sample for the QDs@EVA film with the QD concentration of 6.2 wt% was prepared by drying a drop of the EVA solution with dispersed QDs on a copper grid with an ultra-thin carbon support film (Oken Shoji, HRC-C10). Mean particle sizes were estimated by 100 individual particles in each TEM image. UV-vis absorption spectra of the QD dispersions were measured with a UV-vis optical absorption spectrometer (V-750, JASCO). Herein, for analyses at the same QD concentration, the net absorbance of the dispersions at 400 nm was adjusted to 0.05. The Tauc plot was calculated in according to eqn (1) to determine the E_g of the QDs.[32]

$$(\alpha h\nu)^2 = A(h\nu - E_g) \quad (1)$$

where α is the absorbance, h is the Planck constant, ν is the frequency, and A is a constant. In-line and total transmission spectra of the film samples and glass plates were measured with a UV-vis optical absorption spectrometer (V-750, JASCO) equipped with a standard film holder (FLH-741, JASCO) and an integrating sphere (ISV-922, JASCO), respectively (see Fig. S3, ESI†). PL and PL excitation (PLE) spectra were recorded using a fluorescent spectrometer (JASCO, FP-8500). Absolute PLQYs were calculated from PL spectra measured with a quantum efficiency measurement system (QE-2000-311C, Otsuka Electronics). Current–voltage (*I*–*V*) curves were measured with a source

measure unit (6242, ADCMT) under AM1.5G simulated solar light (1000 W m^{-2}) generated with a solar simulator (XES-40S1, San-Ei Electric). Incident photon-to-electron conversion efficiency (IPCE) measurements were performed on a source measure unit (B2901A, Keysight Technologies), under light irradiation using a monochromatic light source (MLS-1510, Asahi Spectra). The IPCE of LSC was calculated in according to eqn (2).

$$\text{IPCE}\ (\%) = \frac{n_{\text{out}}}{\Phi_{\text{in}}} \times 100 \qquad (2)$$

where Φ_{in} is the photon flux of the monochromic irradiation incident on the window of LSC and n_{out} is the current through the external circuit. The results of the *I–V* curves and IPCE analyses were the averages of five and three measurements, respectively.

3. Results and discussion

3.1 Characterization of CIS/ZnS QDs

Fig. S4 (ESI†) compares the XRD profile of the QD solid sample with reference data. Each peak was attributed to chalcopyrite-type CIS and sphalerite-type ZnS (ESI†). The observed peaks could not be distinguished because of the close positions of the CIS and ZnS peaks to each other. Fig. S5(A)–(C) (ESI†) shows the FE-TEM image, the fast Fourier transform (FFT) image and the particle size distribution of the QDs (ESI†). There is a gap of a few nm between the nanoparticles, suggesting that OA and DDT are adsorbed on the particle surfaces. The lattice spacing estimated from the spots in the FFT image is 3.0 Å, which is attributed to the (112) plane of chalcopyrite-type CIS and the (111) plane of ZnS. The calculated average particle size was 2.6 ± 0.3 nm.

Fig. S6(A) (ESI†) displays the photographs of the QD dispersion in toluene under white light and 365 nm UV light (ESI†). The transparent samples showed yellow luminescence under UV light excitation. The UV-vis absorption spectrum and corresponding Tauc plot are shown in Fig. S6(B) and (C), respectively (ESI†). The E_g of the QDs was determined to be 2.93 eV, which is larger than 1.53 eV of bulk CIS,[33] indicating the quantum size effect. From the PL spectrum (Fig. S6(D), ESI†), the absolute PLQY of the emission peak at 587 nm (2.11 eV) was calculated to be 61.1%. The overlap between the absorption peak and PL peak is small because of the large Stokes shift, 0.82 eV, calculated from the difference between E_g and the emission energy. The CIS/ZnS QD is excited by interband transition, and shows luminescence through defect levels of Cu vacancy,[26] resulting in the large Stokes shift. This feature of the CIS/ZnS QD suppresses self-absorption of the luminescence and is suitable for LSC applications.

3.2 Optical properties of QDs@EVA films with different QD concentrations

QDs@EVA films with different QD concentrations were prepared with a fixed film thickness of ~0.2 mm. Fig. 1 displays the photographs of the blank EVA (0 wt%) and QDs@EVA films under white light and 365 nm UV light. All films were transparent and colored yellow due to the dispersion of QDs. The yellow fluorescence of QDs was shown under UV light. The in-line and total transmission spectra measured with the standard film holder and the integrating sphere unit are shown in Fig. 2(A) and (B), respectively. In the in-line transmission spectra, the transmittance of QDs@EVA in the whole region significantly decreased with increasing the QD concentration. This might be due to the light scattering loss caused by aggregated particles in the resin. On the other hand, in the total transmission spectra, such a decrease in transmittance was suppressed because scattered light was also collected by the detector. Compared with the UV-vis absorption spectrum of the QD dispersion in Fig. S6(B) (ESI†), the decrease in transmittance of QDs@EVA below ~550 nm is attributed to optical absorption by the QDs (ESI†). Increasing the QD concentration up to 6.2 wt% resulted in a decrease in transmittance, while the change was smaller at the excess concentration, possibly indicating that the QD concentration saturated. The excess QDs might aggregate and precipitate. No large particles visible to the naked eye were observed in the film samples. They were probably removed through the degassing process using the planetary centrifugal mixer. Judging from FE-TEM images in Fig. S7 (ESI†), aggregates of ~100–200 nm were observed along with primary particles dispersed in the resin. The PL spectra are

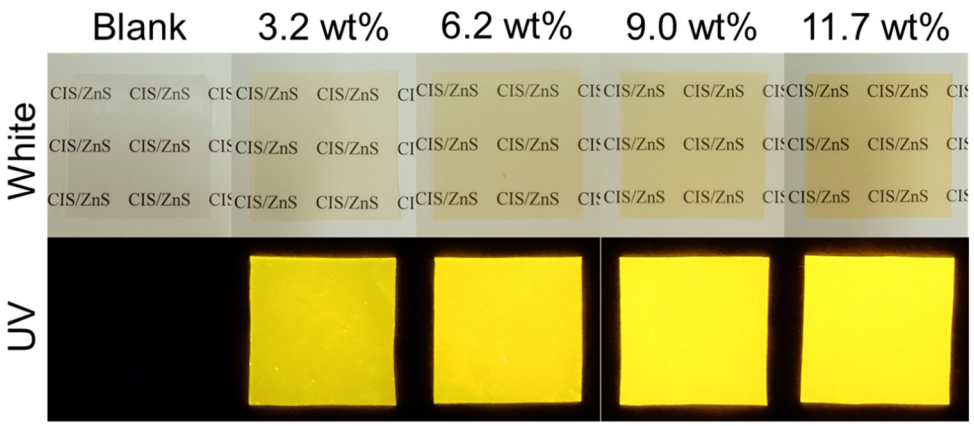

Fig. 1 Photographs of blank EVA film and QDs@EVA at different QD concentrations under white light and 365 nm UV irradiation.

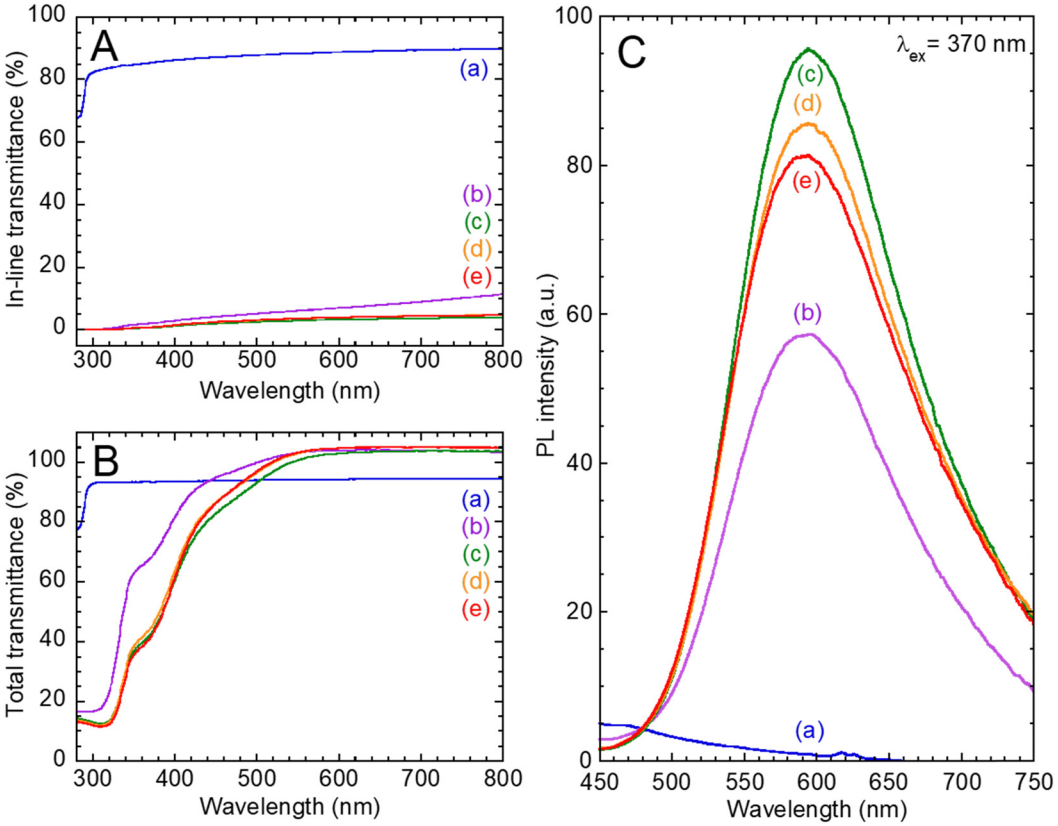

Fig. 2 (A) In-line and (B) total transmission spectra, and (C) PL spectra of film samples at different QD concentrations. (a) Blank EVA, (b) 3.2 wt%, (c) 6.2 wt%, (d) 9.0 wt%, and (e) 11.7 wt%.

shown in Fig. 2(C). In each QDs@EVA, a broad PL peak of the QDs appeared as observed for the QD dispersion (Fig. S6, ESI†). The PL intensity increased with increasing QD concentration up to 6.2 wt%. The decrease at the excess concentration is attributed to concentration quenching. The PLQY of the nanocomposite films were summarized in Table S1 (ESI†). The film with 3.2 wt% exhibited 61.2%, which was close to 61.1% of the QD dispersion in toluene. However, 54.1% was recorded for the film with 11.7 wt%, which was attributed to concentration quenching.

3.3 Change in LSC performance by the QD concentration of QDs@EVA film

The films were attached to the soda glass of the LSC to measure the *I–V* curves under AM1.5G simulated solar light. The obtained short-circuit current (I_{SC}), open-circuit voltage (V_{OC}) and fill factor (*FF*) are summarized in Table S2 (ESI†). As shown in Fig. 3(A), The I_{SC} increased with increasing the QD concentration up to 6.2 wt%, then decreased above (see also Fig. S8, ESI†).

To investigate this change in photocurrent in detail, we measured the IPCE spectra shown in Fig. 3(B). A comparison of the entire spectra revealed that the IPCE reached a maximum at 6.2 wt%, which agreed with the *I–V* curve results. Based on the optical absorption of the QDs, power generation due to PL appears below ~550 nm. The IPCE increased even above ~550 nm, indicating that a part of the incident light scattered from the aggregated QDs reached the solar module. The IPCE in this region reached a maximum at a QD concentration of 6.2 wt%. The number of aggregated particles increased with increasing QD concentration, and the enhanced light scattering up to 6.2 wt% is considered to have enhanced the IPCE. However, excess light scattering caused optical loss, resulting in the decrease in IPCE above 6.2 wt%. The combined effect of both PL and light scattering contributes to the IPCE in the range of ~400–550 nm. It should be noted that the c-Si solar module used generated little electric power below ~400 nm due to absorption of the encapsulant (see Fig. S2, ESI†). As elastic scattering of light does not change the wavelength, power generation by the scattered incident light almost does not occur in this region. The change in IPCE below ~400 nm therefore should be dominantly affected by the wavelength conversion effect through the PL of QDs@EVA. A monotonical decrease in IPCE with increasing QD concentration was observed below ~400 nm. The PL intensity reached the maximum at 6.2 wt%, as illustrated in Fig. 2(C). This behavior differs from the IPCE result. As the number of aggregated QDs increases, the scattering of luminescence should become more pronounced. Excessive scattering by QDs could probably prevent the collection efficiency of luminescence into the light guide plate. Changes in I_{SC} corresponded to the total behavior of IPCE above 400 nm; IPCE in the region below ~400 nm was low, and its influence was limited due to the low energy in the simulated solar light. From these results, the optimal QD concentration for the LSC was 6.2 wt%.

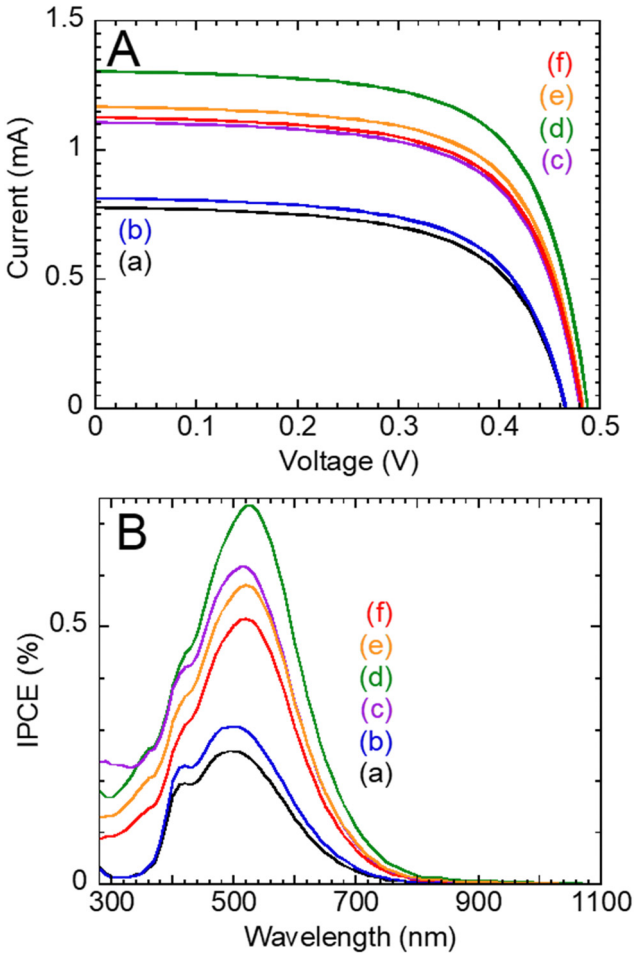

Fig. 3 (A) *I–V* curves and (B) IPCE spectra of the LSC using soda glass plate (a) without and with film samples. (b) Blank EVA and QDs@EVA at (c) 3.2 wt%, (d) 6.2 wt%, (e) 9.0 wt%, and (f) 11.7 wt%.

The LSCs without the film and with the blank EVA film generated a photocurrent, revealing that some of the incident light reached the solar module. A comparison in the *I–V* curves and IPCE spectra shown in Fig. 3 demonstrated that usage of the blank EVA film slightly improved the power generation performance. The role of the EVA resin is to protect the QDs, provide processability and flexibility, and suppress concentration quenching. Its high transparency in the near-UV and visible regions, as shown in Fig. 2(A), suggests that the PL of QDs was not prevented and that there was low light scattering loss from EVA. However, the comparison in the photovoltaic properties indicates that light scattering by the EVA film contributed more to the power generation, possibly due to residual crystallinity of the resin.

3.4 Change in LSC performance by thickness of QDs@EVA film

The QDs@EVA films were prepared with varying thicknesses, with the QD concentration fixed at the optimized 6.2 wt%. Fig. 4 exhibits the photographs of the QDs@EVA films with thickness of 79–373 μm under white light and UV light. All films were uniform and crack-free. The in-line and total transmission spectra are shown in Fig. 5(A) and (B). In-line transmission spectra showed that the transmittance of the QDs@EVA decreased significantly in the whole region as the film thickness increased. The absorption peak of the QDs did not clearly appear due to the significant light scattering loss. On the other hand, the total transmission spectra showed an increase in optical absorption of the QDs below ~550 nm. The change in PL spectra is shown in Fig. 5(C). The PL intensity increased with increasing film thickness, reaching a maximum at 324 μm. It slightly decreased at 373 μm, possibly because of optical loss due to excessive light scattering.

The films were attached to the soda glass of the LSC to measure the *I–V* curve under simulated sunlight. The results are summarized in Table S3 (ESI†). As shown in Fig. 6(A), I_{SC} increased with increasing thickness up to 324 μm then decreased above (see also Fig. S9, ESI†). When thickness was 324 μm, I_{SC} increased by a 1.71-fold compared to without film. The change in the IPCE spectrum is illustrated in Fig. 6(B). When thickness was 324 μm, area of the IPCE spectrum increased by a 3.58-fold compared to without film. The IPCE above ~550 nm, where the QDs had no optical absorption, was maximum at 324 μm, revealing that the effect of light scattering by aggregated QDs increased with increasing film thickness. The IPCE decreased at 373 μm due to the reduced optical collection efficiency into the LSC system by excessive light

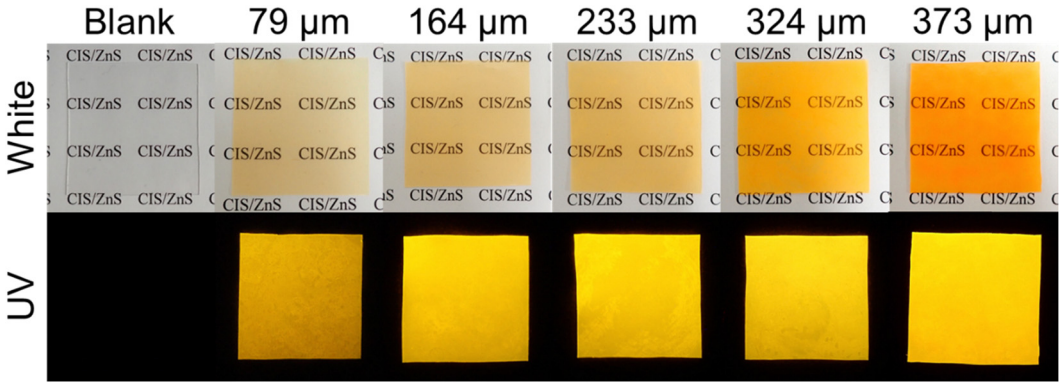

Fig. 4 Photographs of blank EVA film and QDs@EVA with different thicknesses under white light and 365 nm UV light.

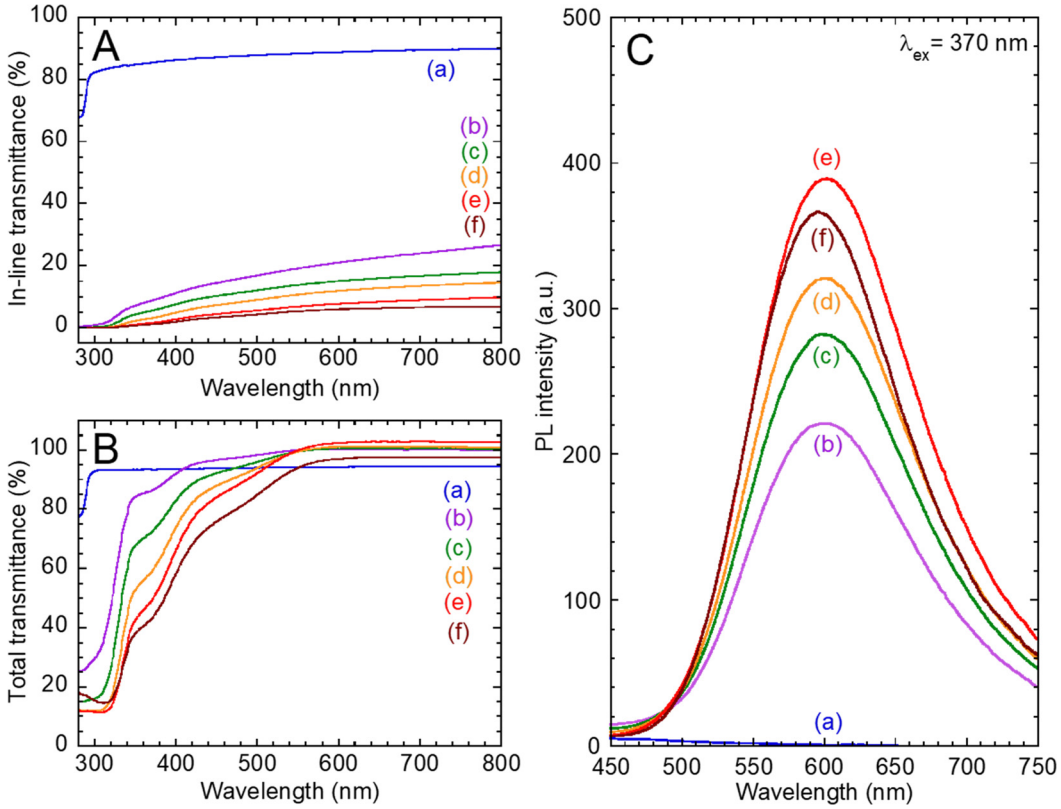

Fig. 5 (A) In-line and (B) total transmission spectra, and (C) PL spectra of (a) blank EVA film and QDs@EVA with film thickness of (b) 79 μm, (c) 164 μm, (d) 233 μm, (e) 324 μm, and (f) 373 μm.

scattering. As mentioned above, the change in IPCE below ~400 nm was attributed to the wavelength conversion effect of QDs, while the combined effect of both PL and light scattering appeared in the range of ~400–550 nm. The IPCE below ~400 nm exhibited a decrease trend with increasing film thickness, whereas the PL intensity reached its maximum at 324 μm. The enhanced light scattering loss for luminescence with greater film thickness resulted in a reduction in the PL collection efficiency into the light guide plate. The change in I_{SC} by film thickness corresponded to the behavior of IPCE above 400 nm. This is analogous to the results varying the QD concentration discussed in the Section 3.3. From these results, the optimal film thickness for the LSC was 324 μm.

Table 1 shows a comparison of the soda glass-based LSCs using nanophosphors in our previous reports adopting the same characterization method as in this study. All of the nanophosphors were dispersed in EVA resin. ΔI_{sc} represents the rate of relative change in I_{sc} with respect to that of LSC without film sample. The ΔI_{sc} of the LSC of the $CuGaS_2$/ZnS QDs was 77.7%, larger than the 71.0% of this study.[28] The absorption edge of the QDs was on the shorter wavelength side and absorbed less sunlight than the CIS/ZnS QDs. However, the higher PLQY and the shorter wavelength PL peak with less absorption by the soda glass would be responsible for the larger ΔI_{sc}. $CsPbCl_3$:Er^{3+},Mn^{2+} QDs had small self-absorption and high PLQY, whereas the ΔI_{sc} was only 14.9%.[15] The primary reason for the low power generation performance is that the fabrication conditions of the nanocomposite film were not optimized for the LSC application in the work. Furthermore, in comparison with the CIS/ZnS QDs, the absorption edge appeared on the shorter wavelength, and the PL peak was observed at the longer wavelength. The smaller amount of absorbed sunlight and the more significant absorption loss of PL by the light guide plate would also contribute to the small ΔI_{sc}. The absorption edge and the PLQY of *p*-phenylenediamine carbon dots were close to those of CIS/ZnS QDs.[34] The PL peak at shorter wavelengths was considered to be less affected by absorption by the light guide plate. However, the ΔI_{sc} was only 16.6%, probably attributed to the significant self-absorption loss resulting from the large overlap between the absorption and PL peaks of the carbon dots.

3.5 Influence of optical absorption by light guide plate on the LSC performance

Soda glass has considerable optical absorption attributed to the presence of impurity ions. To investigate the effect of optical absorption by the light guide plate on the power generation performance, LSCs were fabricated using soda glass and low-absorption glass (white glass) plates. Fig. 7(A) shows their *I*–*V* curves under the simulated solar light. The measurement results are summarized in Table S4 (ESI†). When the optimized QDs@EVA film with the QD concentration of 6.2 wt% and the

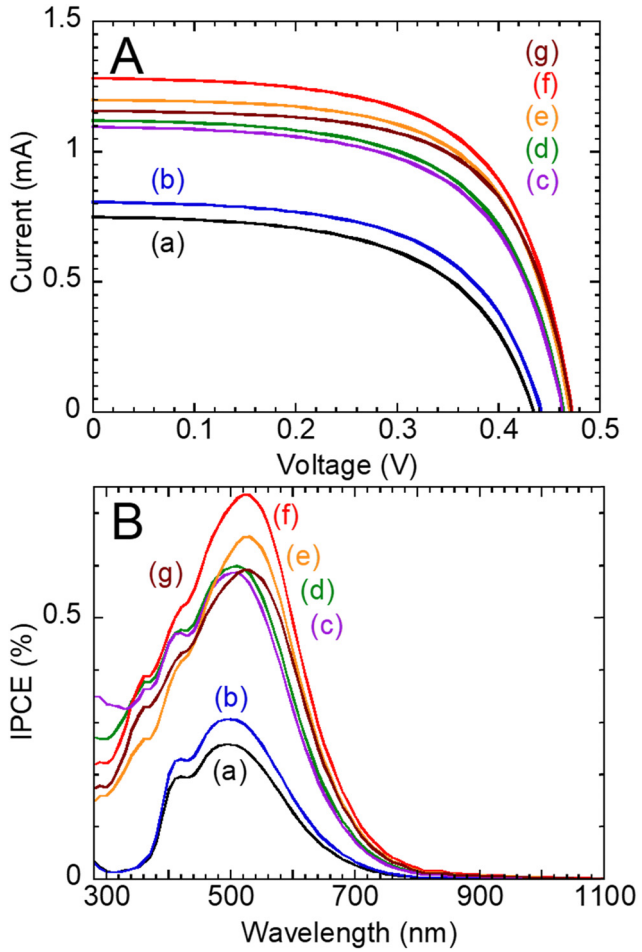

Fig. 6 (A) *I–V* curves and (B) IPCE spectra of the LSC using soda glass plate (a) without and with film samples. (b) blank EVA and QDs@EVA with film thickness of (c) 79 μm, (d) 164 μm, (e) 233 μm, (f) 324 μm, and (g) 373 μm.

film thickness of 324 μm was attached to the soda glass-based LSC, the I_{SC} increased from 0.806 mA to 1.281 mA. On the other hand, the I_{SC} for the white glass-based LSC changed from 2.651 mA to 5.000 mA. The introduction of white glass into LSC led to a fourfold increase of I_{SC} compared to the use of soda glass. The IPCE spectra are shown in Fig. 7(B). The behavior below ~400 nm for the soda glass-based LSC without film sample was similar to the original spectrum of the c-Si solar module used (see Fig. S2, ESI†). However, the IPCE exhibited a significant decrease from ~500 nm to longer wavelengths. Notably, no power generation was negligible in the near-infrared region above 800 nm. In contrast, the white glass-based LSC generated electric power even in the near-infrared region. These results are attributed to the difference in optical absorption characteristics of the light guide materials. Fig. 7(C) shows the transmission spectra of the light guide plates used. The white glass displayed no optical absorption in the visible and the near-infrared regions, whereas the soda glass exhibited significant decrease in transmittance. The decline of IPCE above ~500 nm indicates that the optical absorption by the soda glass prevented PL and scattered incident light from reaching the solar module.

It should be noted that the white glass-based LSC showed photocurrent generation below ~320 nm even without the QDs@EVA. This photoelectric conversion was caused by the intrinsic PL of the white glass. Fig. 7(D) shows the PL and PLE spectra of the light guide plates used. The white glass exhibited a higher PL intensity than the soda glass plate. The similarity between the IPCE and PLE spectra below ~320 nm indicates that the intrinsic PL of the white glass generated the photocurrent. The IPCE was eventually enhanced across the entire region when QDs@EVA was attached through both wavelength conversion and light scattering effects by the QDs.

3.6 Comparison by film position on LSC

When the LSC is used for windows, the QDs@EVA film is placed on the indoor side of the glass plate, considering the excellent weather resistance of the glass plate. Incident light must reach the QDs@EVA film after significant optical absorption by the glass plate. To investigate this absorption influence, LSCs with two windows at front and rear sides were fabricated (see Fig. S10, ESI†). The method of LSC preparation except for the window was the same as in 2.4. The power generation performance was measured by changing the film positions. *I–V* curves and their summary are shown in Fig. 8(A) and Table S5 (ESI†), respectively. Regardless of the glass material used, a larger photocurrent was obtained when the nanocomposite film was placed on the rear side of the glass plate. The IPCE spectra of the LSCs exhibited in Fig. 8(B) also showed an entire increase in IPCE when the nanocomposite film was positioned on the rear side. This may be attributed to the PL and back-scattered light from the film sample being more efficiently confined within the LSC system. However, a decrease in the IPCE was observed below ~330 nm for the soda glass-based LSC, indicating that the incident UV light was prevented from reaching the QDs@EVA at the rear side due to strong absorption by the soda glass plate.

Table 1 Comparison with the previous results of the soda glass-based LSCs using nanophosphors which were evaluated in the same way

Nanophosphor	Absorption edge (nm)	Main PL peak (nm)	PLQY (%)	ΔI_{sc} (%)	Ref.
CIS/ZnS QD	~550	587	61.1	71.0	This work
$CuGaS_2$/ZnS QD	~450	568	73	77.7	28
$CsPbCl_3:Er^{3+},Mn^{2+}$ QD	~410	~600	79.5	14.9	15
p-PD derived CD	~540	~540	56	16.6	34

p-PD: *p*-phenylenediamine; CD: carbon dot.

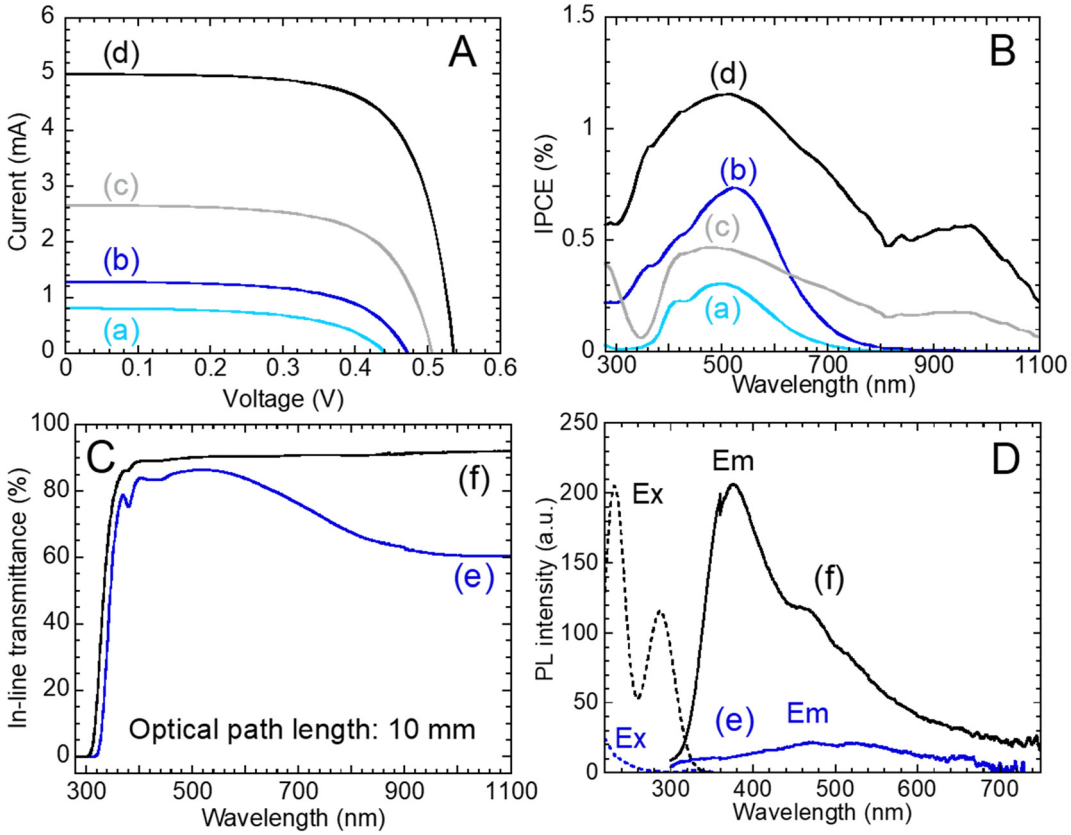

Fig. 7 (A) *I*–*V* curves and (B) IPCE spectra of the LSCs using (a), (b) soda glass and (c), (d) white glass plates with (a), (c) blank EVA film and (b), (d) the optimized QDs@EVA film. (C) In-line transmission spectra and (D) PL and PLE spectra of the (e) soda glass (λ_{ex} = 220 nm, λ_{em} = 476 nm) and (f) white glass (λ_{ex} = 233 nm, λ_{em} = 377 nm) plates.

Based on the above, when soda glass is used as the light guide plate, the absorption of impurity ions dramatically reduces the power generation characteristics. However, the cost of glass materials increases as the impurity ion concentration is reduced. The use of soda glass is unavoidable for the widespread use of the LSC as the building material. To suppress the effect of absorption by soda glass, it is desirable to use the QD that exhibits a narrow PL peak around 520 nm, because the soda glass absorbs light above 520 nm, as shown in Fig. 7(C). CIS/ZnS QD has tunable PL wavelength in the visible region and small self-absorption due to the large Stokes shift,[35–37] while these QDs show a broad defect-related PL peak; therefore, further work is needed to reduce the PL peak width for minimizing absorption by the glass plate.

4. Conclusions

In this research, the influence of the light absorption by the soda glass on the LSC using CIS/ZnS QDs was investigated. CIS/ZnS QDs were synthesized by the hot injection method and dispersed in EVA to prepare the QDs@EVA films. These films were combined with the soda glass plate and the c-Si solar module to fabricate the LSCs. The QD concentration and film thickness were optimized for the LSC performance. Increasing the QD concentration up to 6.2 wt% enhanced the photocurrent due to increased effects of PL and light scattering. However, beyond this concentration, strong light scattering due to QD aggregation reduced the photocurrent. The film thickness also affected the effects of PL and light scattering on the LSC performance. The photocurrent was maximized at the thickness of 324 μm. When the optimal QDs@EVA film was applied to the LSC, the I_{SC} and the IPCE spectrum area could be increased by a 1.71-fold and 3.58-fold compared to without film, respectively. For the control, a white glass plate with low optical absorption was used in LSC. The LSC with white glass exhibited a fourfold increase in I_{SC} compared to the LSC with soda glass. This improvement was attributed to more PL and scattered incident light reaching the solar module due to the low optical absorption of the light guide plate. Furthermore, the photocurrent was increased by relocating the film position from the frontside to the rear. This was due to an enhanced confinement efficiency of the PL and backscattered light in the LSC system. The soda glass plate showed absorption for both PL and scattered light in the visible and near-infrared region, resulting in the significant photocurrent loss. To avoid this problem of the soda glass-based LSC, it would be necessary to develop QDs with a narrow emission peak at ~520 nm. The measured photovoltaic properties are dependent on the geometry of the

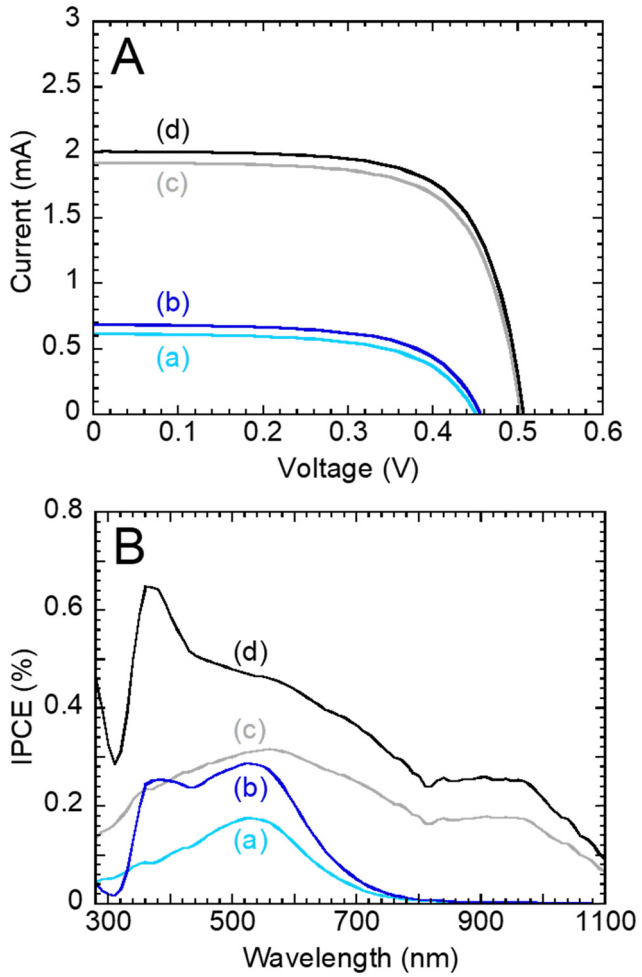

Fig. 8 (A) *I–V* curves and (B) IPCE spectra of the LSCs using (a), (b) soda glass and (c), (d) white glass plates with the optimized QDs@EVA film at the (a), (c) front and (b), (d) rear sides.

LSC. However, the influence of soda glass absorption should be a common problem. In addition to the PL properties, durability is also a significant consideration. Further evaluation of photostability, *e.g.* by accelerated tests, will be necessary for the long-term practical application of LSCs with QD nanocomposite films and a soda glass plate.

Author contributions

Y. Imakiire: formal analysis, investigation, methodology, writing – original draft; Y. Iso: conceptualization, funding acquisition, project administration, supervision, writing – review and editing; T. Isobe: supervision, writing – review and editing. All authors gave final approval for publication and agreed to be held accountable for the work performed therein.

Data availability

The authors declare that all data supporting the results reported in this study are available within the paper and the ESI.† Additional data used for the study are available from the corresponding authors upon reasonable request.

Conflicts of interest

There are no conflicts to declare.

Acknowledgements

This research was supported by the Izumi Science and Technology Foundation, the Mazda Foundation, the Iketani Science and Technology Foundation and the Yashima Environment Technology Foundation.

References

1 M. Hughes, D. Borca-Tasciuc and D. Kaminski, *Sol. Energy Mater. Sol. Cells*, 2017, **171**, 293–301.
2 S. Gallagher, B. Norton and P. Eames, *Sol. Energy*, 2007, **81**, 813–821.
3 H. Liu, S. Li, W. Chen, D. Wang, C. Li, D. Wu, J. Hao, Z. Zhou, X. Wang and K. Wang, *Sol. Energy Mater. Sol. Cells*, 2018, **179**, 380–385.
4 J. Huang, J. Zhou, E. Jungstedt, A. Samanta, J. Linnros, L. Berglund and I. Sychugov, *ACS Photonics*, 2022, **9**, 2499–2509.
5 M. Fimbres-Romero, A. Flores-Pacheco, M. Alvarez-Ramos, E. Mario and R. Lopez-Delgado, *ACS Omega*, 2024, **9**, 28008–28017.
6 J. Lin, L. Wang, Q. Jing and H. Zhao, *Chem. Eng. J.*, 2024, **481**, 148441.
7 H. Zhao, G. Liu, S. You, F. Camargo, M. Zavelani-Rossi, X. Wang, C. Sun, B. Liu, Y. Zhang, G. Han, A. Vomiero and X. Gong, *Energy Environ. Sci.*, 2021, **14**, 396–406.
8 Y. Iso, S. Takeshita and T. Isobe, *J. Electrochem. Soc.*, 2012, **159**, J72–J76.
9 A. Morimoto, Y. Iso and T. Isobe, *ACS Appl. Mater. Interfaces*, 2024, **16**, 7780–7789.
10 J. Pan, S. Sarmah, B. Murali, I. Dursun, W. Peng, M. Parida, J. Liu, L. Sinatra, N. Alyami, C. Zhao, E. Alarousu, T. Ng, B. Ooi, O. Bakr and O. Mohammed, *J. Phys. Chem. Lett.*, 2015, **6**, 5027–5033.
11 Y. Zhou, H. Zhao, D. Ma and F. Rosei, *Chem. Soc. Rev.*, 2018, **47**, 5866–5890.
12 I. Coropceanu and M. Bawendi, *Nano Lett.*, 2014, **14**, 4097–4101.
13 G. Gu, X. Zhang, Y. Guo, Z. Zheng, X. Cao, Y. Zhang, R. Huang and X. Zhang, *Appl. Phys. Lett.*, 2021, **119**, 011905.
14 J. Bomm, A. Büchtemann, A. Chatten, R. Bose, D. Farrell, N. Chan, Y. Xiao, L. Slooff, T. Meyer, A. Meyer, W. van Sark and R. Koole, *Sol. Energy Mater. Sol. Cells*, 2011, **95**, 2087–2094.
15 P. Song, S. Hase, S. Zhao, Z. Xu, Y. Iso and T. Isobe, *ACS Appl. Nano Mater.*, 2022, **5**, 2522–2531.

16 W. S. Song, J. H. Kim, J. H. Lee, H. S. Lee, H. S. Jang and H. Yang, *Mater. Lett.*, 2013, **92**, 325–329.
17 R. Xie, M. Rutherford and X. Peng, *J. Am. Chem. Soc.*, 2009, **131**, 5691–5697.
18 A. Aboulaich, M. Geszke, L. Balan, J. Ghanbaja, G. Medjahdi and R. Schneider, *Inorg. Chem.*, 2010, **49**, 10940–10948.
19 P. Chuang, C. Lin and R. Liu, *ACS Appl. Mater. Interfaces*, 2014, **6**, 15379–15387.
20 L. Li, A. Pandey, D. Werder, B. Khanal, J. Pietryga and V. Klimov, *J. Am. Chem. Soc.*, 2011, **133**, 1176–1179.
21 D. Pan, L. An, Z. Sun, W. Hou, Y. Yang, Z. Yang and Y. Lu, *J. Am. Chem. Soc.*, 2008, **130**, 5620–5621.
22 L. Lim, X. Zhao and Z. Tan, *Adv. Mater.*, 2023, **35**, 2301887.
23 O. Korepanov, D. Kozodaev, O. Aleksandrova, A. Bugrov, D. Firsov, D. Kirilenko, D. Mazing, V. Moshnikov and Z. Shomakhov, *Nanomater.*, 2023, **13**, 2892.
24 Y. Iso and T. Isobe, *ECS J. Solid State Sci. Technol.*, 2020, **9**, 016005.
25 H. McDaniel, N. Fuke, N. Makarov, J. Pietryga and V. Klimov, *Nat. Commun.*, 2013, **4**, 2887–2896.
26 B. Chen, H. Zhong, W. Zhang, Z. Tan, Y. Li, C. Yu, T. Zhai, Y. Bando, S. Yang and B. Zou, *Adv. Funct. Mater.*, 2012, **22**, 2081–2088.
27 Y. Nakamura, Y. Iso and T. Isobe, *ACS Appl. Nano Mater.*, 2020, **3**, 3417–3426.
28 S. Hase, Y. Iso and T. Isobe, *J. Mater. Chem. C*, 2022, **10**, 3523–3530.
29 M. Kastelijn, C. Bastiaansen and M. Debije, *Opt. Mater.*, 2009, **31**, 1720–1722.
30 M. Bergren, N. Makarov, K. Ramasamy, A. Jackson, R. Guglielmetti and H. McDaniel, *ACS Energy Lett.*, 2018, **3**, 520–525.
31 A. Velarde, E. Bartlett, N. Makarov, C. Castañeda, A. Jackson, K. Ramasamy, M. Bergren and H. McDaniel, *ACS Appl. Energy Mater.*, 2020, **3**, 8159–8163.
32 J. Tauc and A. Menth, *J. Non-Cryst. Solids*, 1972, **8–10**, 569–585.
33 R. Yan, W. Zhang, W. Wu, X. Dong, Q. Wang and J. Fan, *APL Mater.*, 2016, **4**, 126101.
34 Y. Liu, Y. Iso and T. Isobe, *J. Mater. Chem. C*, 2025, **13**, 786–792.
35 J. Hua, Y. Du, Q. Wei, X. Yuan, J. Wang, J. Zhao and H. Li, *Physica B*, 2016, **491**, 46–50.
36 R. Zhang, P. Yang and Y. Wang, *J. Nanopart. Res.*, 2013, **15**, 1910.
37 B. Huang, R. Xu, L. Zhang, Y. Yuan, C. Lu, Y. Cui and J. Zhang, *J. Mater. Chem. C*, 2017, **5**, 12151–12156.

